

Detectors in Particle Physics

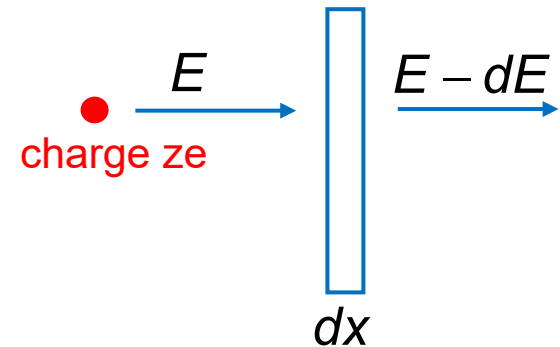
1. Interactions of particles and radiation with matter (recap)
2. Tracking detectors, vertexing and magnetic spectrometer
3. Calorimeters
4. Particle identification
5. Detector systems

1. Interactions of particle and radiation w/ matter

Energy loss of heavy charged particles:

($m > m_e$)

Energy loss of particles from ionization of matter atoms through collisions with shell electrons.



Average specific energy loss dE/dx described by Bethe-Bloch formula

$$\left\langle \frac{dE}{dx} \right\rangle_{\text{ion}} = - \underbrace{\left(\rho N_A \frac{Z}{A} \right)}_{n_e} 4\pi r_e^2 m_e c^2 z^2 \cdot \frac{1}{\beta^2} \cdot \left(\ln \frac{2m_e c^2 \gamma^2 \beta^2}{I} - \beta^2 \right)$$

ρ = density

N_A = Avogadro number

Z, A = charge and mass number

r_e = class. Electron radius

I = effective ionization energy

z = charge of the projectile

β = velocity of the projectile

$$r_e = \frac{e^2}{4\pi m_e c^2}$$

To reduce the material dependence one often divides the specific energy loss by the material density

$$\left\langle \frac{dE}{dx} \right\rangle \rightarrow \left\langle \frac{1}{\rho} \frac{dE}{dx} \right\rangle$$

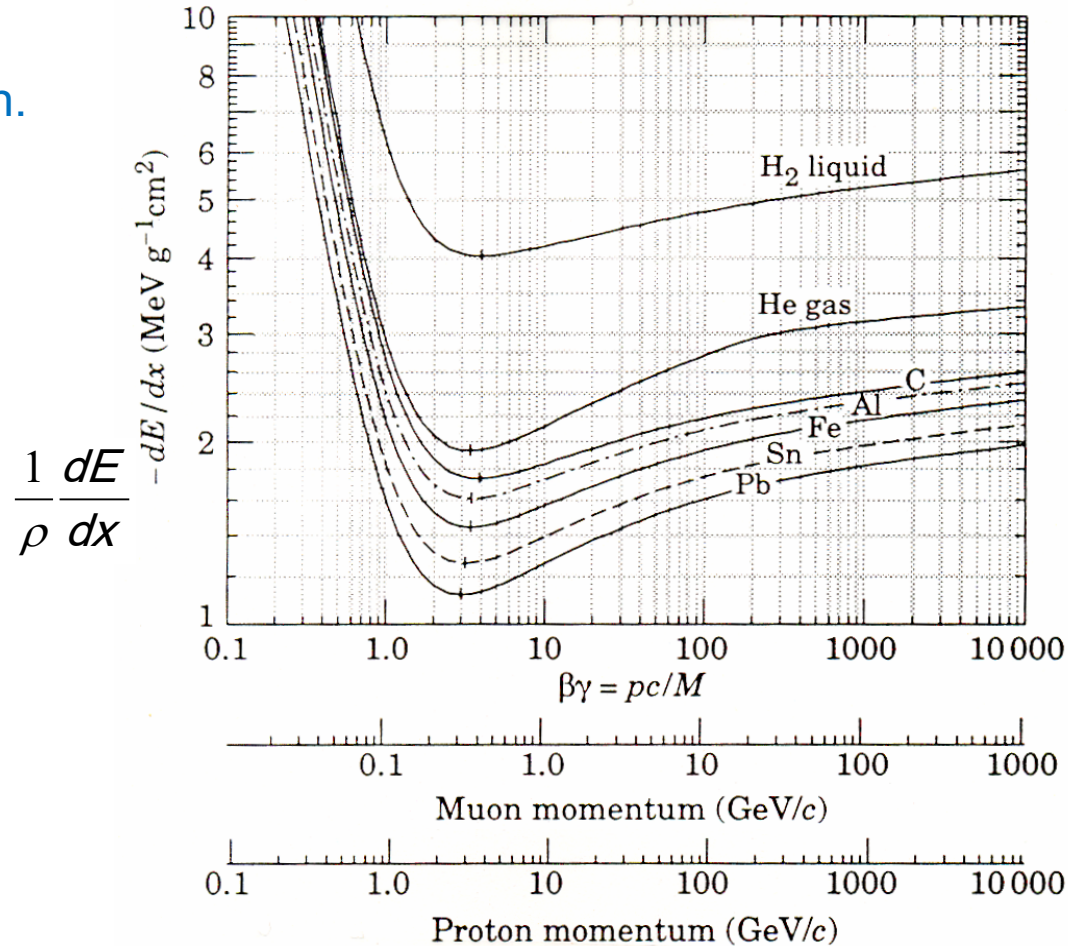
(this is often hidden by redefining the $\rho x \rightarrow x'$)

$$\frac{1}{\rho} \left\langle \frac{dE}{dx} \right\rangle = - \underbrace{(N_A 4\pi r_e^2 m_e c^2)}_K z^2 \frac{Z}{A} \cdot \frac{1}{\beta^2} \cdot \left(\ln \frac{2m_e c^2 \gamma^2 \beta^2}{I} - \beta^2 \right)$$

$$K/A = 0.307 \text{ MeV g}^{-1} \text{ cm}^2 \text{ mit } A = 1 \text{ g} \cdot \text{Mol}^{-1}$$

w/ $Z/A \approx 0.5$ for most materials: $K Z/A \approx 0.150 \text{ MeV g}^{-1} \text{ cm}^2$

Energy loss through ionization.



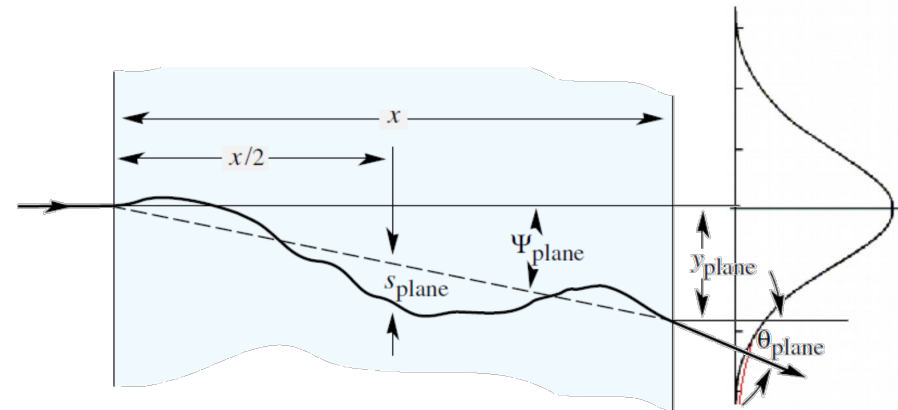
Plot from PDG

difference: Z/A

- $\sim 1/\beta^2$ for small $\beta\gamma$
- Minimum at $\beta\gamma = 3\dots 4$ w/ $dE/dx = 1\dots 2 \text{ MeV g}^{-1} \text{ cm}^2$ (multiply with ρ to get dE/dx): if one ignores Bremsstrahlung (for muons up to $\beta\gamma = O(1000)$ i.e. 100 GeV) particles are quasi “minimal ionizing” also above $\beta\gamma$ of 3.
- For small $\beta\gamma$, dE/dx can be used for particle ID (see below)

Multiple scattering:

Multiple collisions of the projectile with the atoms of the material (stochastic process) leads to a deflection of the particle



For small angles the deflection follows a Gaussian distribution, at least for the central 98%.

The widths of the Gaussian can be approximated. Depending if one measures the deflection in a plan or in space one obtains:

One finds that the width parameter θ_0 depends on the path x through the material in units of the radiation length X_0 and on the particle's momentum. It is less for high momentum particles.

$$\frac{1}{\sqrt{2\pi} \theta_0} \exp \left(-\frac{\theta_{\text{plane}}^2}{2\theta_0^2} \right)$$

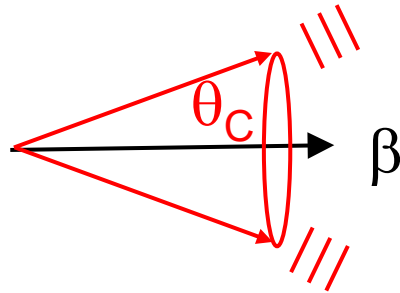
$$\theta_0 = \theta_{\text{plane}}^{\text{rms}} = \frac{1}{\sqrt{2}} \theta_{\text{space}}^{\text{rms}}$$

$$\theta_0 = \frac{13.6 \text{ MeV}}{\beta c p} z \sqrt{\frac{x}{X_0}}$$

Cherenkov-radiation:

When a particle traverses a medium with a velocity β (particle velocity β close to c for highly relativistic particles) which is larger than the speed of light within that medium, the particle emits Cherenkov radiation (threshold $\beta > 1/n$).

Cherenkov radiation is emitted on a cone with an opening angle θ_c



$$\cos \theta_C = \frac{1}{\beta n}$$

Emitted photons are ranging from the visible blue spectrum to the ultraviolet and The number of photons per unit length of the radiator and per wave-length unit is

$$\frac{d^2 N_\gamma}{dx d\lambda} = \frac{2\pi\alpha z^2}{\lambda^2} \left(1 - \frac{1}{\beta^2 n(\lambda)^2} \right) \quad \text{z is the charge of the particle.}$$

Medium must be transparent: gases (\rightarrow Ring-Cherenkov counter) or water (e.g. large water Cherenkov detectors used for neutrino detection).

Energy loss of electrons (positrons)

For light electrons there are two mechanism competing:

- Energy loss through ionization (essentially a la Bethe-Bloch, but max. momentum transfer much larger: $\Delta E = 1/2 E_{\text{kin}}$ & identical particles!)
- Energy loss through Bremsstrahlung

$$\left\langle \frac{dE}{dx} \right\rangle = \left\langle \frac{dE}{dx} \right\rangle_{\text{ion}} + \left\langle \frac{dE}{dx} \right\rangle_{\text{Brems}}$$

For high-energy electrons the energy loss by Bremsstrahlung is by far dominating. Only for very low-energy electrons the energy loss by ionization takes over.

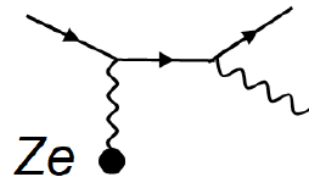
Critical energy E_c :

$$\left\langle \frac{dE}{dx} \right\rangle_{\text{ion}} \Big|_{E_c} = \left\langle \frac{dE}{dx} \right\rangle_{\text{Brems}} \Big|_{E_c}$$

One finds empirically for solid materials: $E_c \approx 610 \text{ MeV} / (Z + 1.2)$

Remark: for lead, bremsstrahlung dominates above $\sim 10 \text{ MeV}$

Bremsstrahlung:



Typical length scale for Bremsstrahlung:
Radiation length X_0 :

$$\frac{1}{X_0} = \rho N_A \frac{Z^2}{A} \cdot 4\alpha \cdot r_e^2 \cdot \ln \left(\frac{183}{Z^{1/3}} \right)$$

(strong Z dependence)

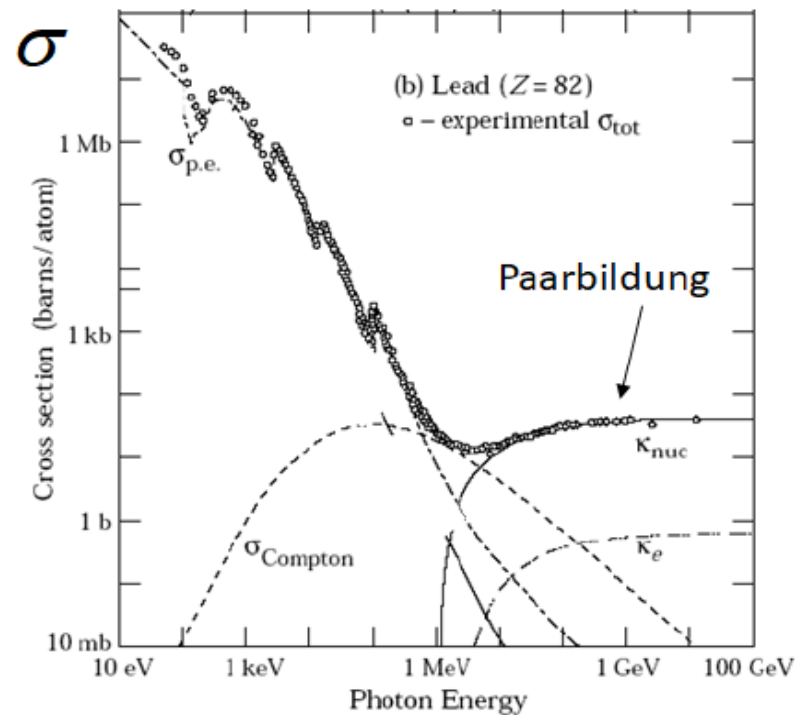
Energy loss:

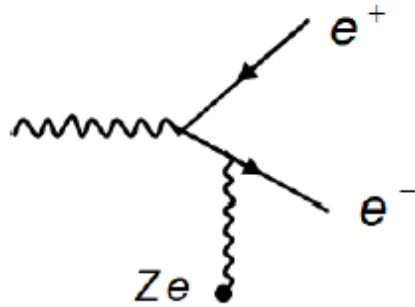
$$\left\langle \frac{dE}{dx} \right\rangle_{\text{Brems}} \approx -\frac{1}{X_0} E$$

Energy loss of photons

Photons interact in different ways with matter. Most relevant mechanisms:

- Photo-electric effect for low energy photons
- Compton effect for photon energies between 10 KeV and MeV
- Pair production for $E_\gamma > 1 \text{ MeV}$ ($2m_e$)



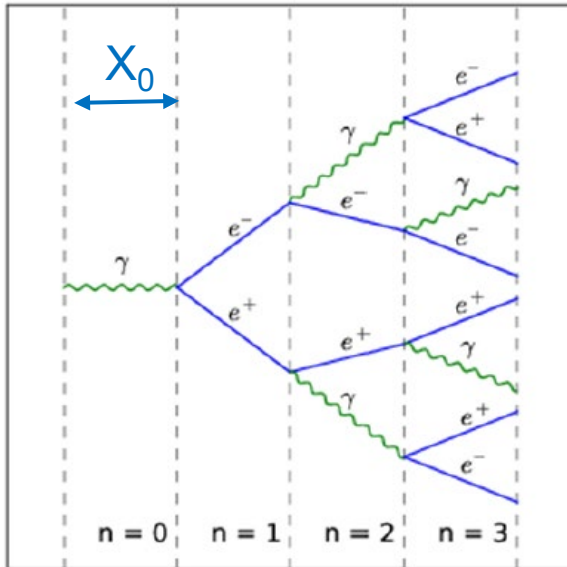


The typical length scale for pair production in matter is again the radiation length.
An exact calculation however results into $9/7 X_0$ - slightly larger than for bremsstrahlung) (both processes w/ similar Feynman diagrams)

Cross section is largely constant: $\sigma = \frac{7}{9}(A/X_0 N_A)$

Electromagnetic shower

Simple shower model for higher-energy photons/electrons.
 Electrons/photons make bremsstrahlung / pair production after $\sim X_0$



In every step the number of shower particles is doubled: $N(t) = 2^t$

The average energy of the shower particles is E/N – the shower stops when the particle energy has reached the critical energy E_c in the material:

Max. shower depth: $t_{\max} = \frac{\ln(E / E_c)}{\ln 2}$

With increasing energy E of the detected particle the calorimeter depth should increase with $\sim \ln(E / E_c)$

$$E / 2^{t_{\max}} = E_c$$

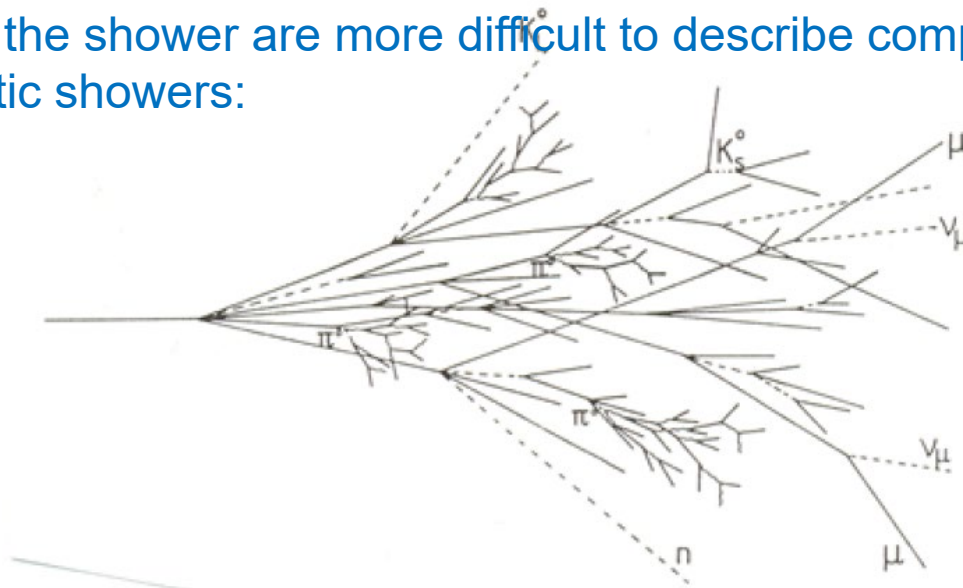
$$\rightarrow \ln(E / E_c) = t_{\max} \ln 2 =$$

Hadronic shower

High-energy hadrons ($E \gg 1$ GeV) interact with the nuclei and the nucleons of the matter and produce a shower of secondary particles.

$$n, p, \pi^\pm, K^\pm, K^0 + A \longrightarrow \text{Shower of secondary particles}$$

The details of the shower are more difficult to describe compared to electromagnetic showers:



Characteristic interaction length (λ_{int}) for hadron passing matter is given by:

$$\lambda_{\text{int}} = \frac{1}{n \cdot \sigma_{\text{int}}} = \frac{A}{\rho N_A} \cdot \frac{1}{\sigma_{\text{int}}}$$

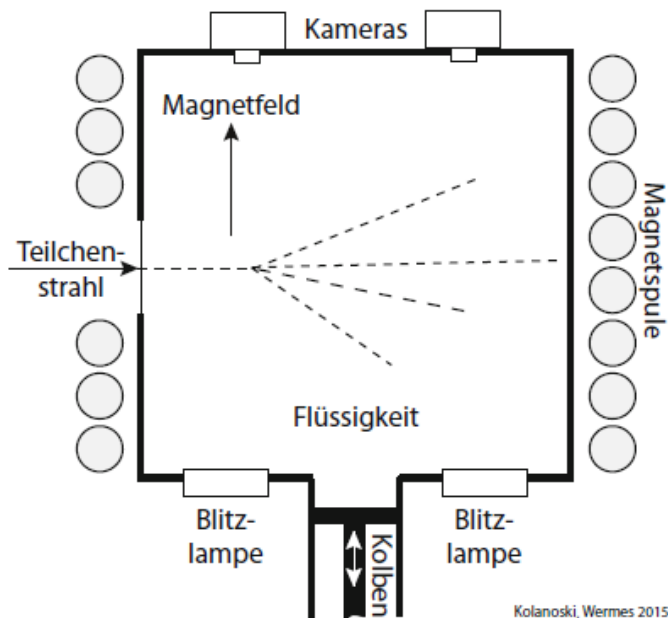
Element	λ_{int}
Fe	16.8 cm
Pb	17.6 cm
C	39 cm

Where one finds empirically $\sigma_{\text{int}} \approx 35 \text{ mb } A^{0.7}$

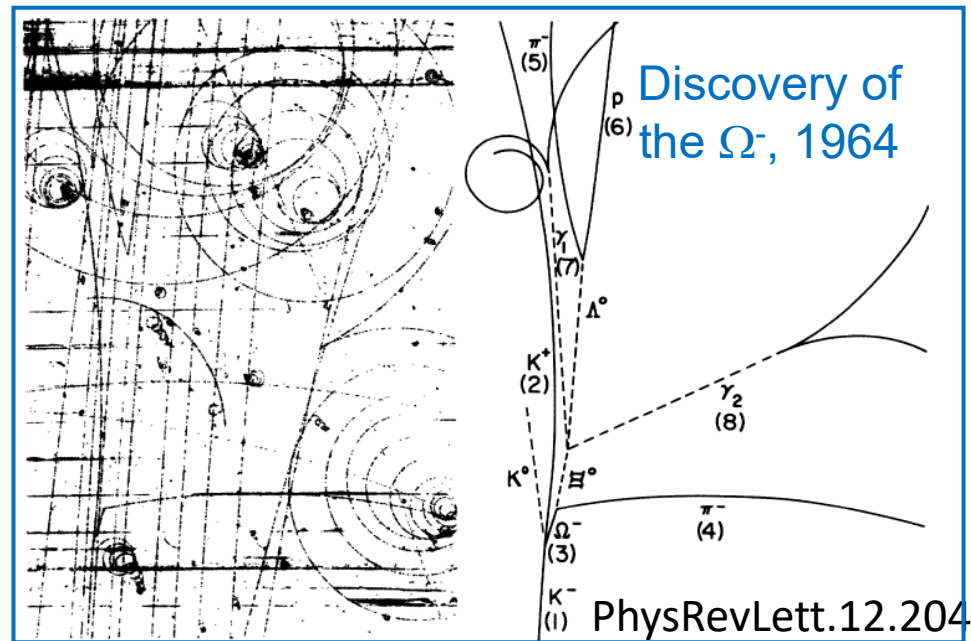
2. Tracking, vertexing and magnetic spectrometer

Reconstruct track of charged particle in an magnetic field → use the track curvature to estimate the momentum → reconstruct decay vertices.

Historical example: **Bubble chamber** (by D. Glaser in 1952, Nobel prize in 1960)



Kolanoski, Wermes 2015



vessel filled with a superheated transparent liquid (often H_2).

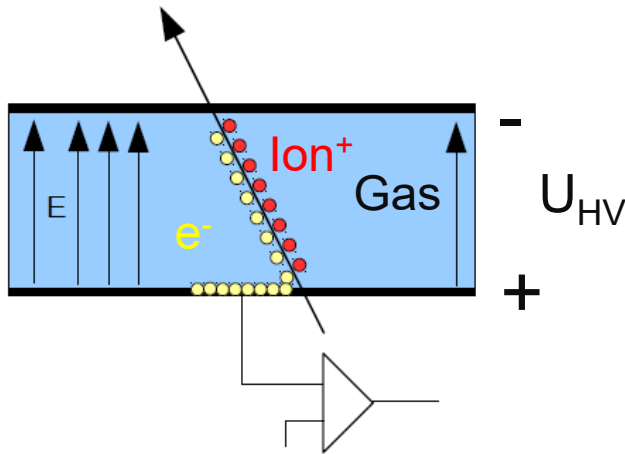
Reconstruction of tracks, decay vertices, momenta. Disadvantage: photo w/ subsequent digitization, heavy piston to arm the detector

Multi-wire proportional chambers (MWPCs)

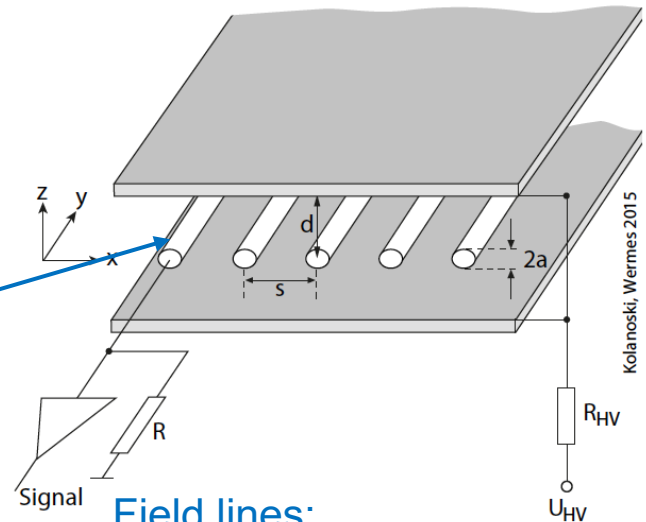
Georges Charpak (1968), Nobel prize in 1992.

Wire chambers have revolutionized charged particle detection: fully electronic event recording, high data acquisition rates (up to 40 MHz), excellent position resolution when operated as drift chambers.

Detection principle:

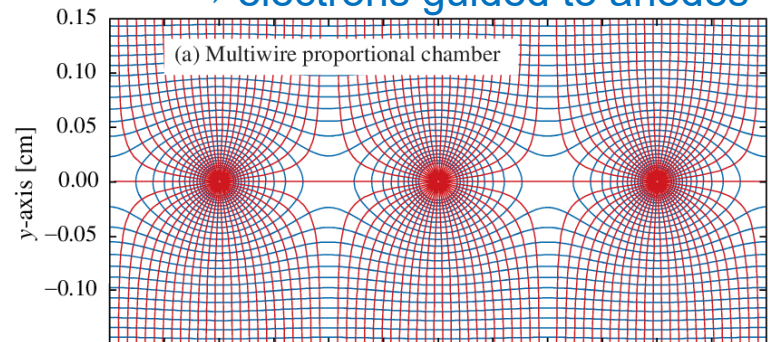


Thin anode wires – gas amplification



Field lines:

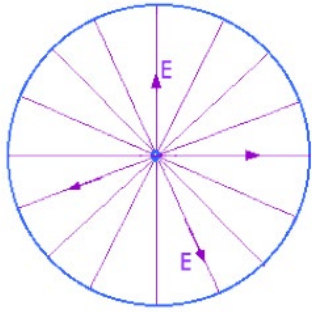
→ electrons guided to anodes



Charge particle ionizes the gas.
Electrons drift towards the anode.
For wire chambers, the anodes are realized by thin wires → amplification due to strong field.
Electronic processing of signal

Gas amplification:

Wire inside tube:



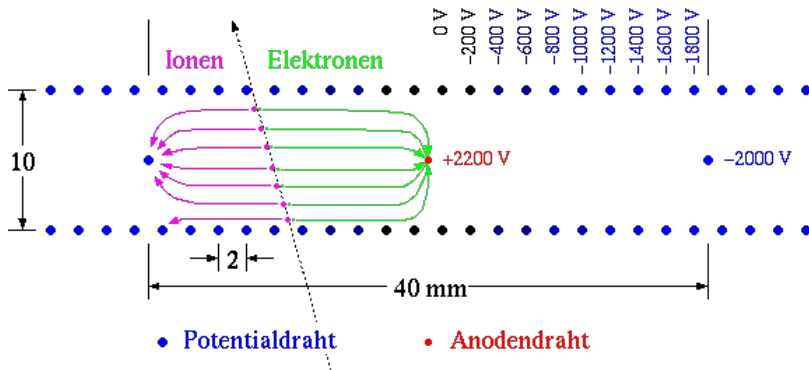
$$E(r) = \frac{U}{r \ln \frac{b}{a}}$$

b = radius of tube
a = radius of wire



Strong electrical field near the wire leads to acceleration of primary electrons and to further ionization → avalanche: gas amplification. Typ. gain $\sim 10^5$

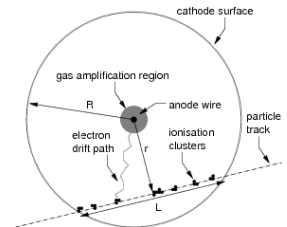
Drift-chambers:



Drift chamber principle was found first in Heidelberg (Physikalisches Institut, by A. H. Valenta).

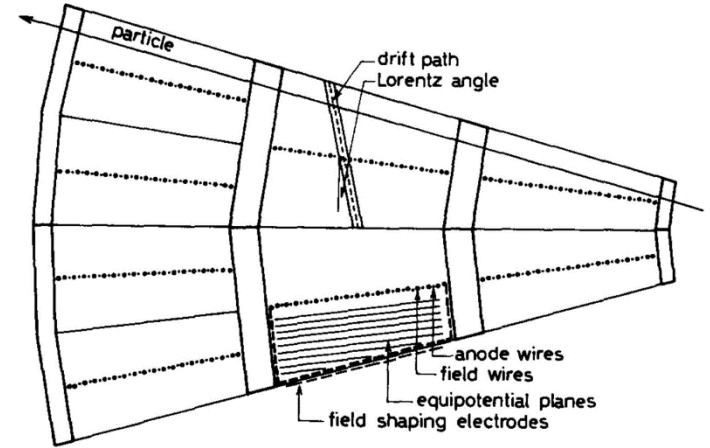
Using special wire configurations one can construct “drift cells” with very homogenous drift paths → one can use the drift time to reconstruct the particle trajectory.

Instead of building drift cells from complicated wire configurations simple tubes with an anode wire can be used:

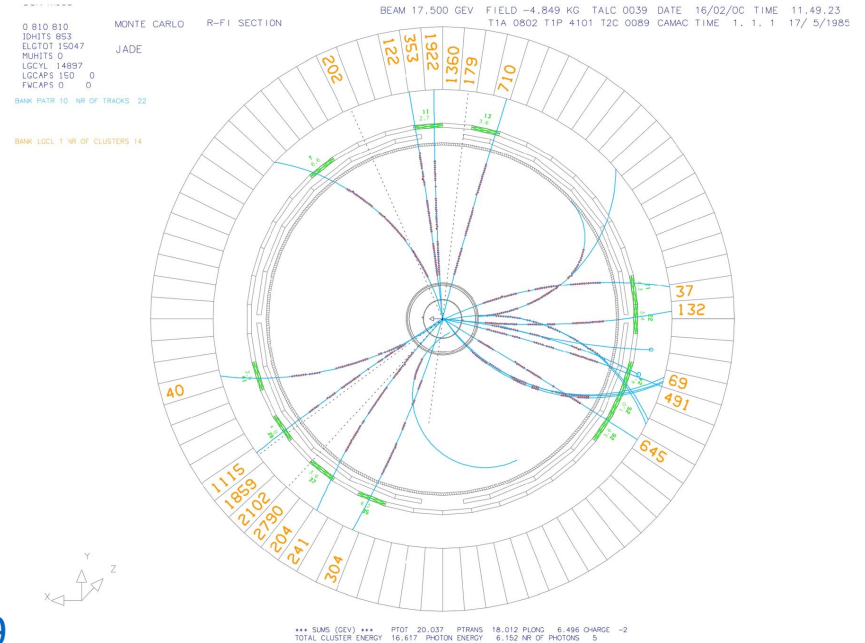


Example 1: JADE Jet-Chamber

Inner Radius: 20cm
 Outer Radius: 80cm
 Length: 2.4m



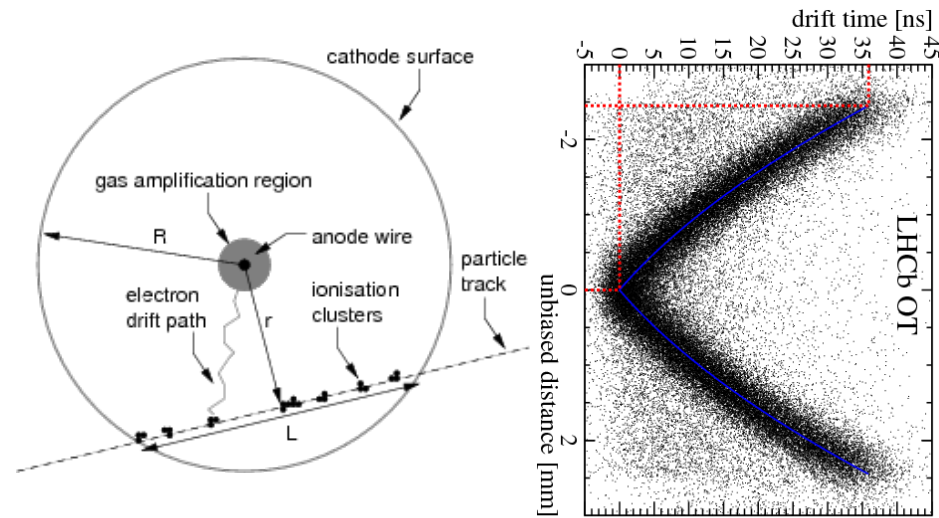
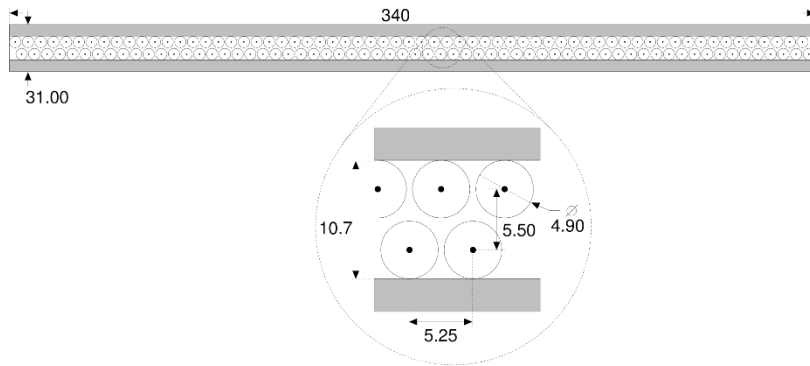
Spatial resolution r_{ϕ} : 170 μm



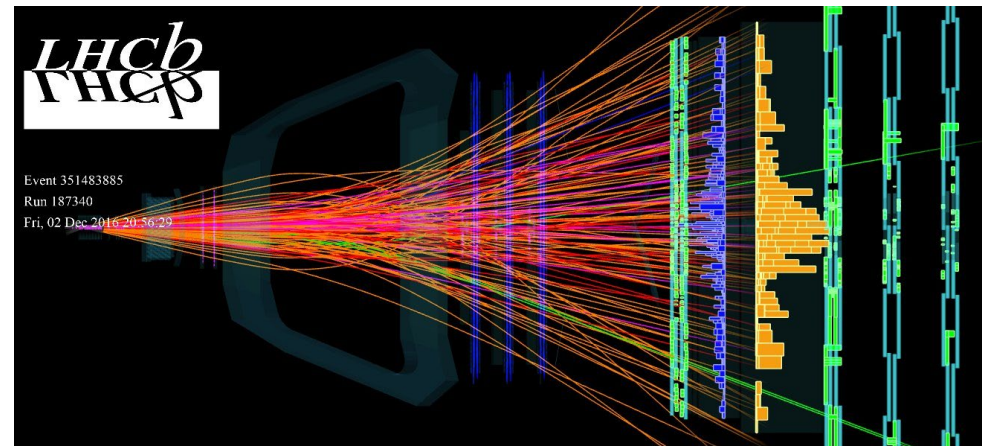
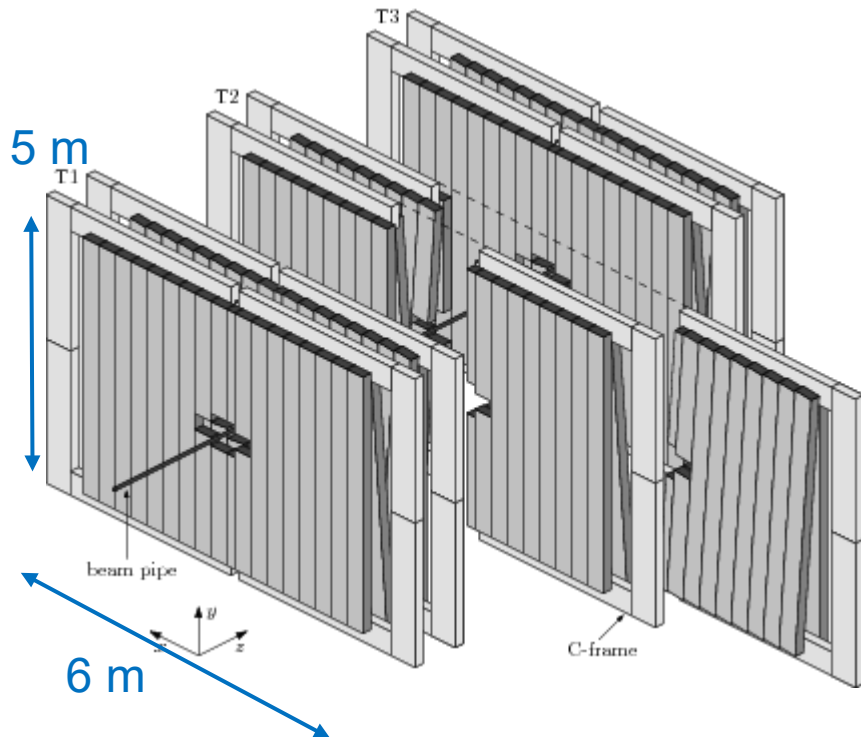
J. Heintze et al.

[https://doi.org/10.1016/0029-554X\(82\)90658-9](https://doi.org/10.1016/0029-554X(82)90658-9)

Example 2: LHCb Outer Tracker

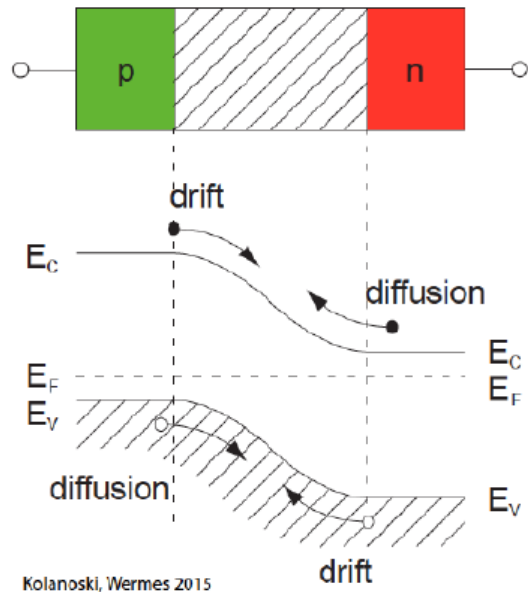


170 μm resolution over
360 m^2 detection areas



Semiconductor strip & pixel detectors

Semiconductor detector – based on depleted np-junctions (diodes)

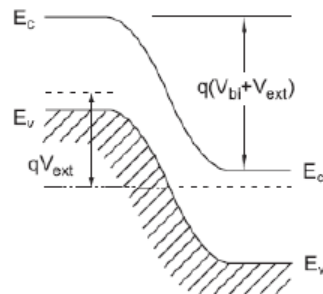
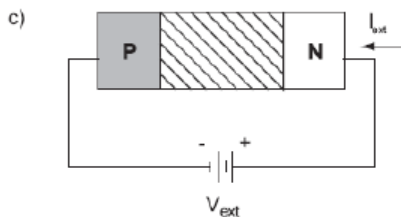


In the junction of p(n) doped semiconductors, the majority charge carriers will diffuse into the other region until the Fermi level is equalized.

Around the junction, there is a region w/o free charge carriers: depletion zone. A space charge is created (pos / neg one n / p-side). The related electrical field produces a drift of charge carriers which compensates the diffusion.

The depletion zone can be enlarged by applying an external voltage:
With p-doping larger than n-doping, the depletion zone extends mostly into n:

Size of depletion zone:

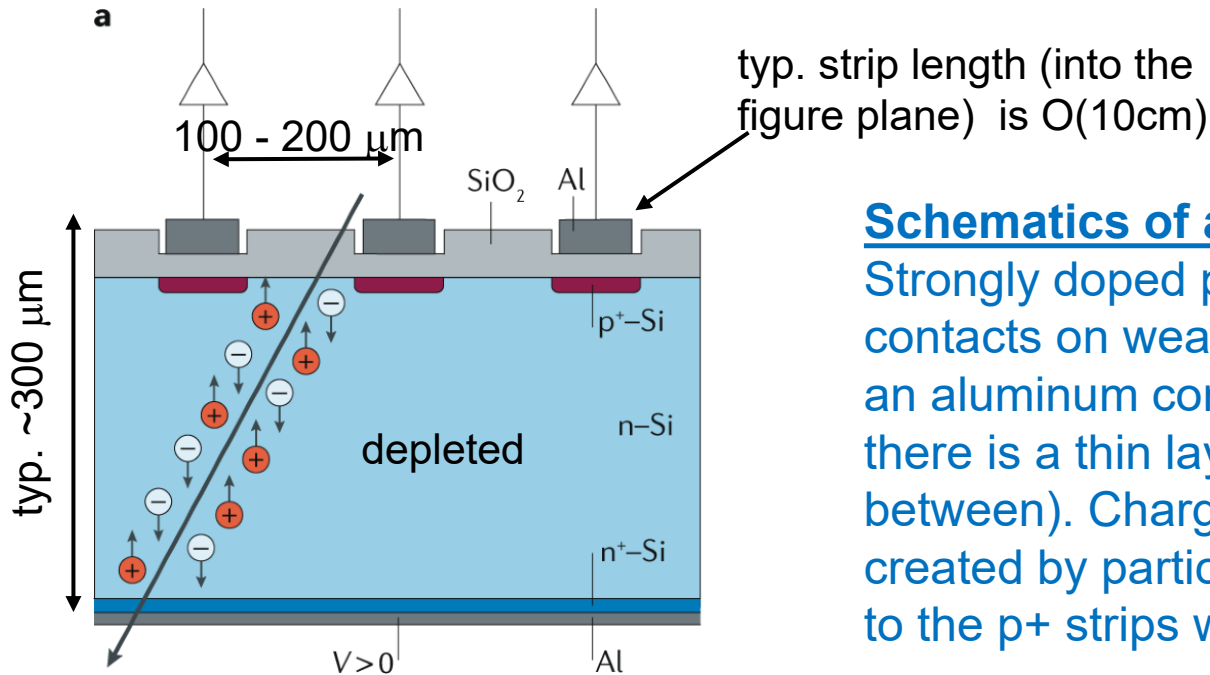


$$d \approx x_n \approx \sqrt{\frac{2\epsilon\epsilon_0}{e} \frac{1}{N_D} (U_{bin} + U_{ext})}$$

$$\approx 3.6 \cdot 10^3 \sqrt{\frac{U_{ext}}{N_D(\text{V cm})}}$$

~300 μm
reachable

“reverse biasing”



Schematics of a silicon strip sensor:

Strongly doped p⁺-strips w/ aluminum contacts on weakly doped n-bulk which has an aluminum contact (by technical reasons there is a thin layer of strongly doped Al in between). Charge carriers (electrons) created by particles drift in the applied field to the p⁺ strips where they are detected.

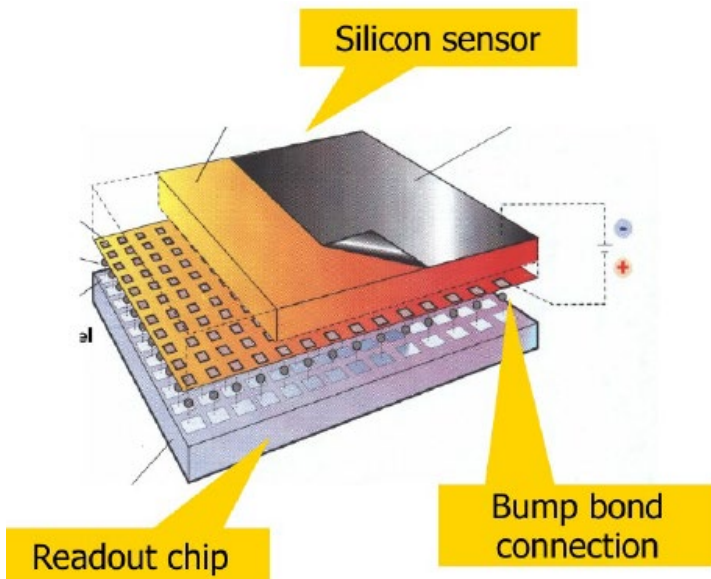
Schematics of a pixel sensor:

Instead of strips one uses small pixels typ. size 50 x 200...400 μm^2 .

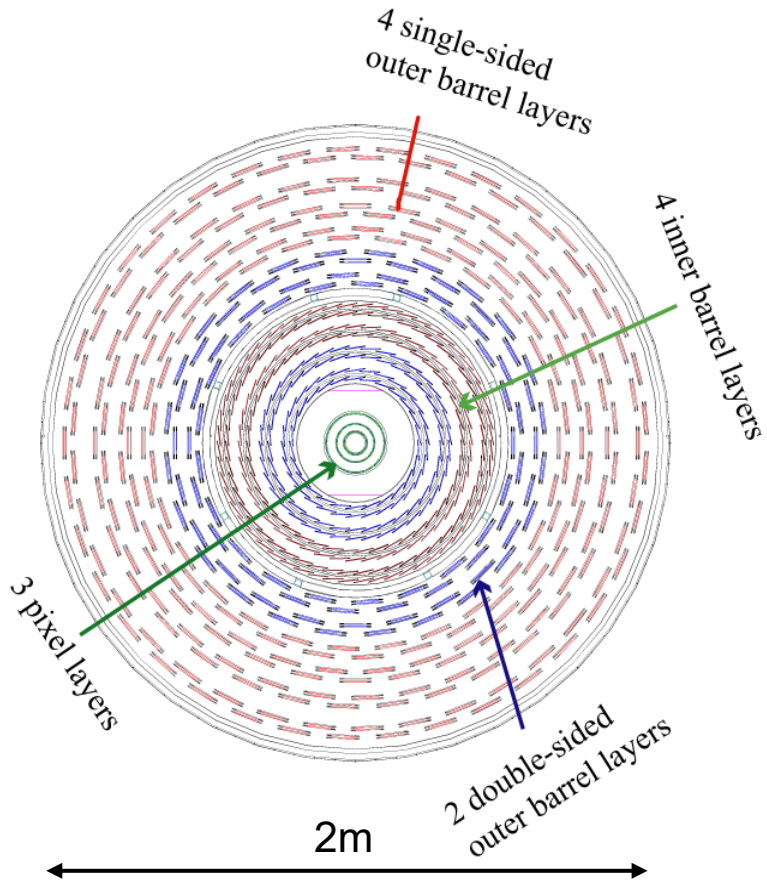
Challenge: Readout of the individual channels (please don't conclude from your mobile camera – these devices are really very slow) . Requires a readout chip bonded on top of the pixel: Hybrid pixel detectors.

Novel development: Monolithic pixel sensors with part of electronics in pixel.

(→Heidelberg: Mu3ePix and MightyPix).



Example 1: CMS Tracker



Silicon Pixel detector:

about 66 million $100 \times 150 \mu\text{m}^2$ pixels arranged at distance of 4 to 11 cm

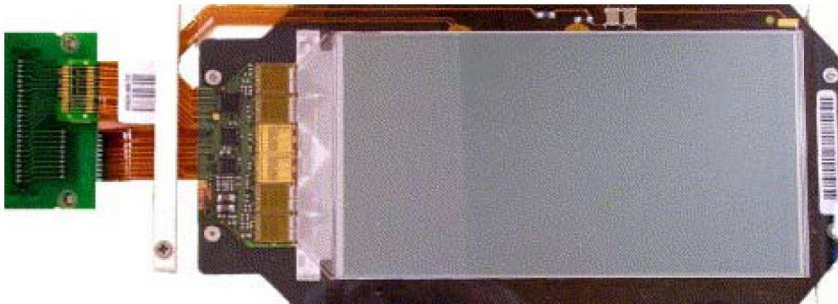
Silicon strip detectors:

divided in the inner barrel part (TIB), the inner disks (TID), the outer barrel (TOB) and outer end-caps (TEC).

Tracker contains 15,200 sensitive modules with a total of about 10 million detector strips.

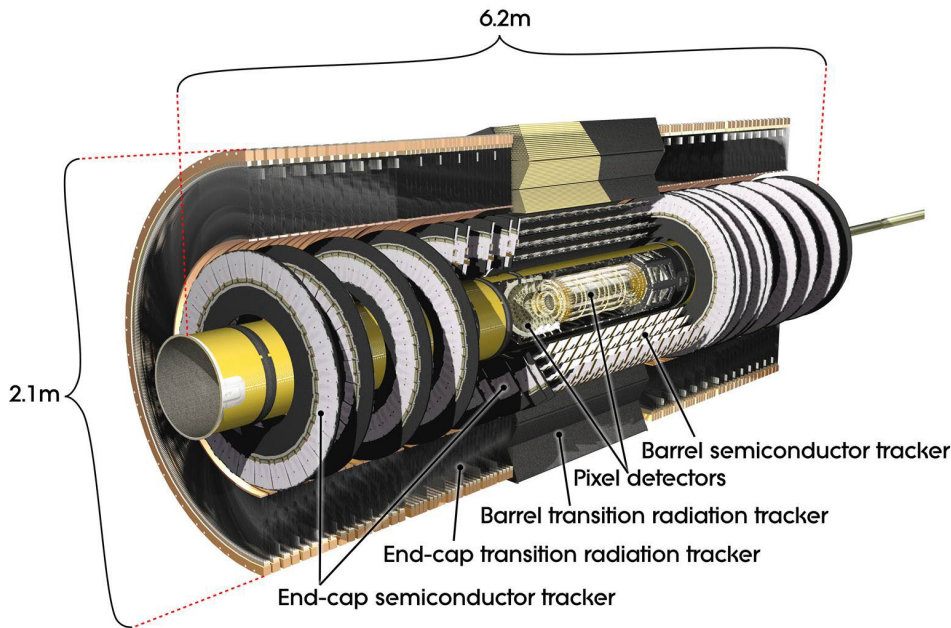
Strip distance = $80 \mu\text{m}$ to $200 \mu\text{m}$
w/ strip widths about 25%

Spatial resolution: $20 - 30 \mu\text{m}$



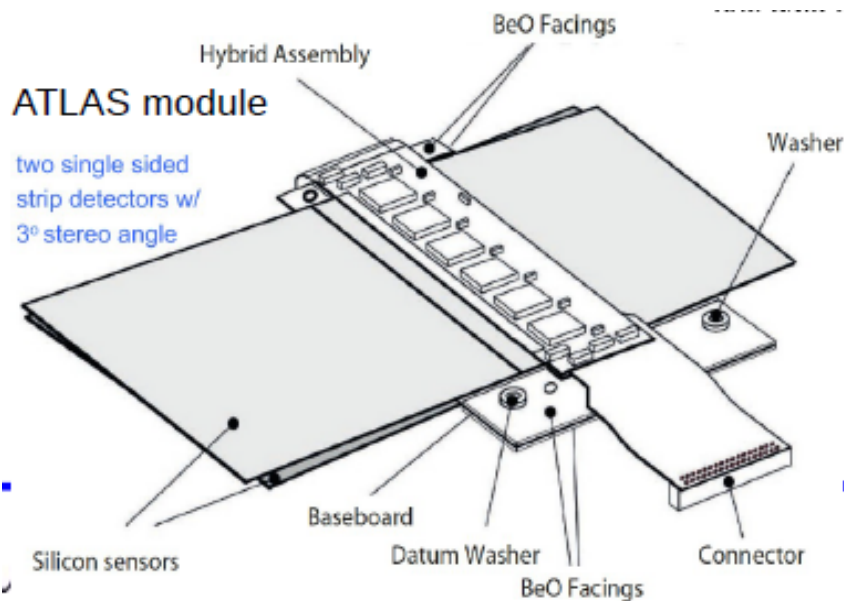
CMS TIB silicon strip modules.

Example 2: ATLAS Inner Tracker



ATLAS pixel detector:

- 92 million pixels (92 million electronic channels).
- Silicon area approx. 1.9m^2
- Pixel $50 \times 400\mu\text{m}^2$ and $50 \times 250 \mu\text{m}^2$ for outer / inner external
- 4-barrel layers with 1736 modules
- 3 disks per end-cap w/ 288 modules
- Typ. Spatial resolution: $10 \mu\text{m}$



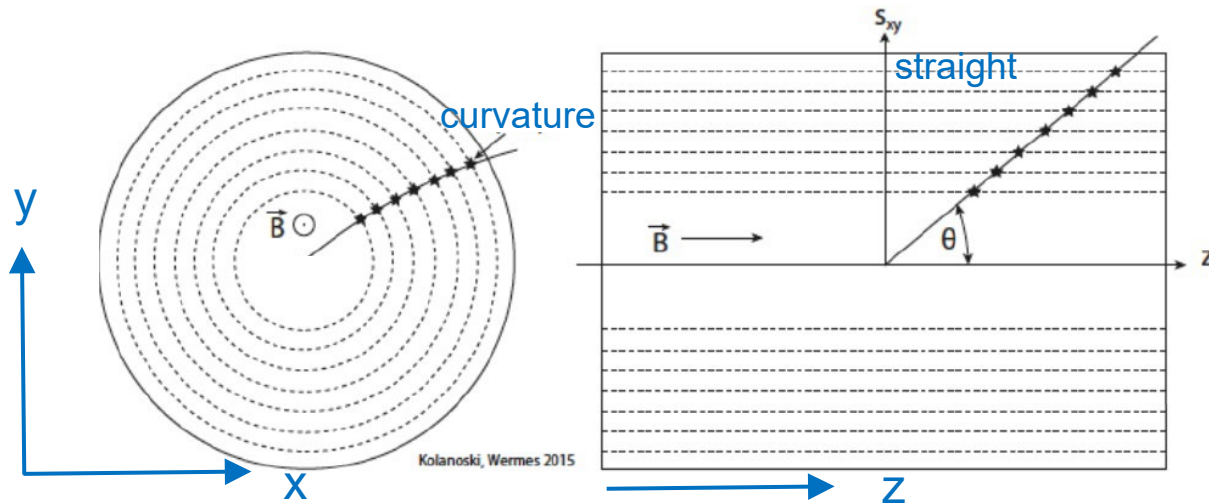
ATLAS strip detector:

4,088 two-sided modules and over 6 million implanted readout strips (6 million channels)
 60m^2 of silicon distributed over 4 cylindrical barrel layers and 18 planar endcap discs
Readout strips every $80\mu\text{m}$.

Typ. spatial resolution: $25 \mu\text{m}$

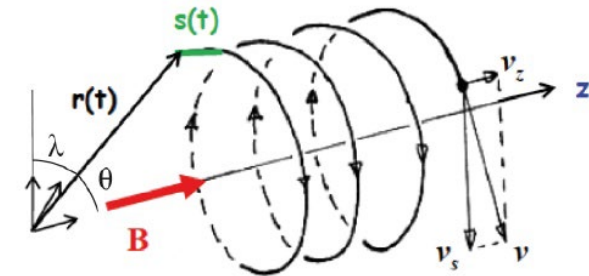
Momentum measurement and B field configurations

B-field (perpendicular w/ measurement plane)



Lorentz force:

$$\vec{F}_{Lorentz} = q (\vec{v} \times \vec{B})$$



Particle moves on a helical trajectory

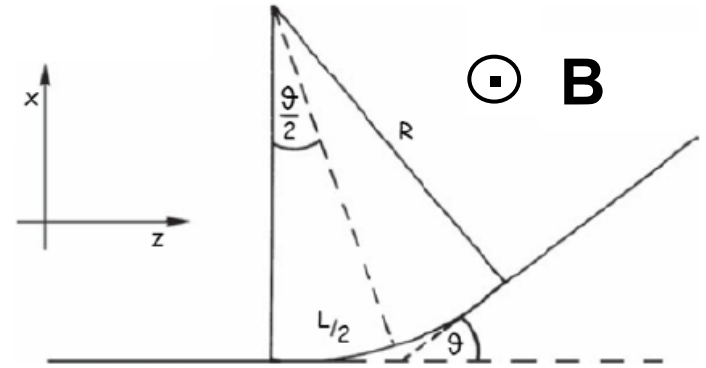
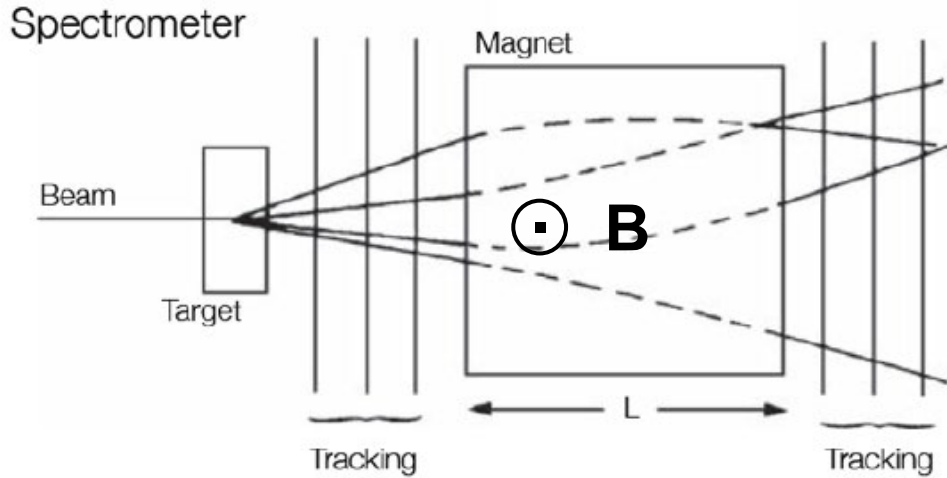
Curvature $1/R$ in xy-plane and particles transverse momentum p_T (within xy plane):

$$p_{\perp} = q \cdot B \cdot R \quad \text{or} \quad p_{\perp} [\text{GeV}] = 0.3 \cdot B [\text{T}] \cdot R [\text{m}]$$

The momentum of the particle is obtained from $p = p_T / \cos \theta$

.How well can the transverse momentum be measured? What is its error?

Forward spectrometer configuration (fixed target exp. or forward experiments
e.g. LHCb)



Minimum spectrometer configuration: 2 tracking station before and after magnet
3rd station is used for redundancy, fake rejection

Deflection angle $\theta \approx \frac{L}{R} = \frac{L}{p} eB \rightarrow p = \frac{eBL}{\theta} = \frac{0.3B[\text{T}]L[\text{m}]}{\theta}$
(p is p_T)

$$\rightarrow dp = \frac{eLB}{\theta^2} d\theta = \frac{p}{\theta} d\theta \rightarrow \frac{dp}{p} = \frac{d\theta}{\theta}$$

Relative momentum resolution is given by relative angular resolution (depends on spatial resolution of tracker)

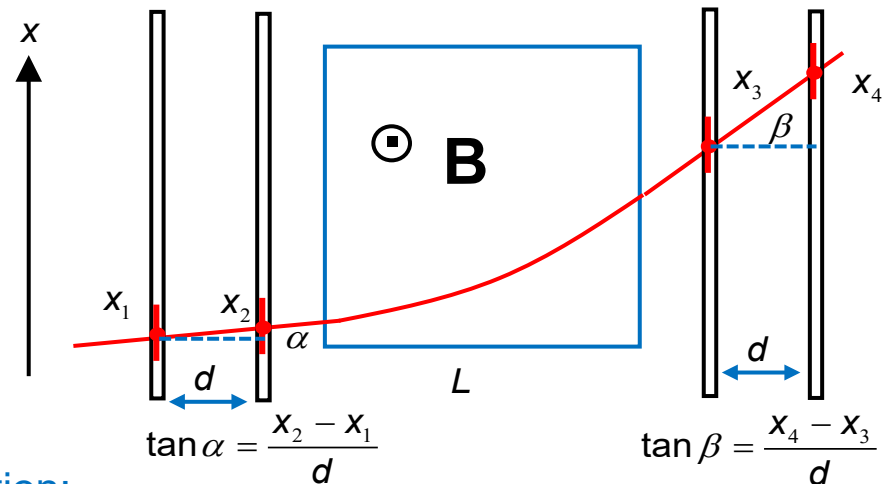
Deflection results into momentum-kick Δp_x :

$$\Delta p_x = p \sin \theta \approx p \theta = eBL \quad \text{often called bending power}$$

Assume the minimum tracker configuration w/
2 + 2 tracking stations w/ spatial resolution σ_x

deflection $\theta = \beta - \alpha \approx \tan \beta - \tan \alpha$

$$\theta \approx \frac{x_4 - x_3}{d} - \frac{x_2 - x_1}{d}$$



W/ σ_x for all layers, one obtains w/ error propagation:

$$d\theta = \frac{2\sigma_x}{d} \quad \text{and with} \quad \frac{dp}{p} = \frac{d\theta}{\theta}$$

For N points before and after magnet:

$$d\theta = \frac{\sigma_x}{d} \sqrt{\frac{24(N-1)}{N(N+1)}}$$

$$\frac{dp}{p} = \frac{p}{eBL} \frac{2\sigma_x}{d} = \frac{p}{0.3B[T]L[m]} \frac{2\sigma_x}{d}$$

Relative momentum resolution depends on p. Improves for larger field integral BL and larger Measurement "arm" h.

There is also a uncertainty on θ from multiple scattering inside the plane:

$$\sigma_{p,MS} = p \sin \theta_{0,MS} \approx p \theta_{0,MS} = p \cdot \frac{13.6 \text{ MeV}}{\beta p} \sqrt{\frac{L'}{X_0}} = 13.6 \text{ MeV} \sqrt{\frac{L'}{X_0}} \quad \leftarrow \text{all material}$$

Contribution to p resolution results from the comparison w/ p-kick and bending power:

$$\frac{\sigma_{p,MS}}{p} = \frac{\sigma_{p,MS}}{\Delta p_x \text{ p-kick}} = \frac{13.6 \text{ MeV}}{eBL} \sqrt{\frac{L'}{X_0}}$$

Contribution from multiple scattering to relative resolution has no momentum dependence

Momentum resolution considering detector spatial resolution and multiple scattering is given by:

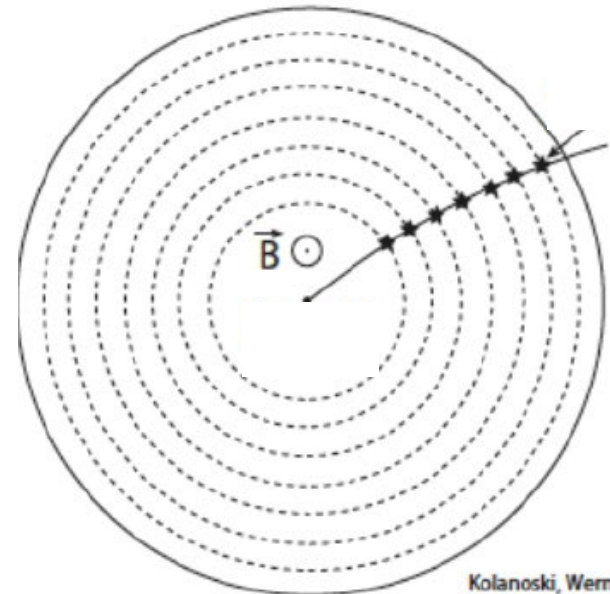
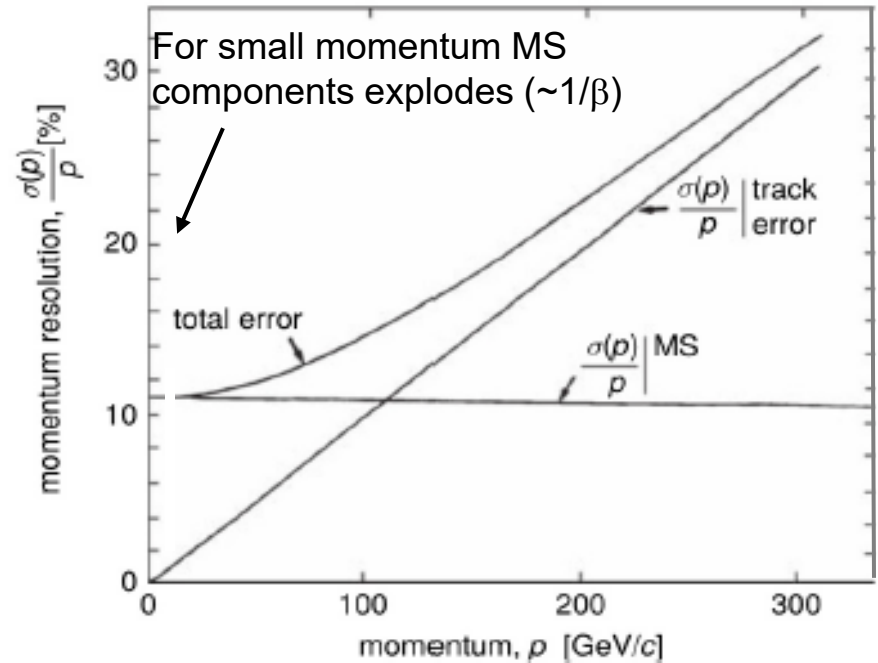
$$\left. \frac{\sigma_{p_T}}{p_T} \right|_{tot} = \sqrt{\left(\left. \frac{\sigma_{p_T}}{p_T} \right|_{det} \right)^2 + \left(\left. \frac{\sigma_{p_T}}{p_T} \right|_{MS} \right)^2}$$

This formula can be applied to more complicated cases – e.g. measurement of the track curvature be cylindrical tracking detector. Assuming the curvature is measured by N space points over distance L one finds for the detector resolution:

$$\left. \frac{\sigma_{p_T}}{p_T} \right|_{det} = \frac{p_T}{0.3 BL^2} \sqrt{\frac{720}{N+4}} \quad \text{for } N \geq 10$$

(B in T, L in m, p in GeV)

(In literature referred as Gluckstern formula)

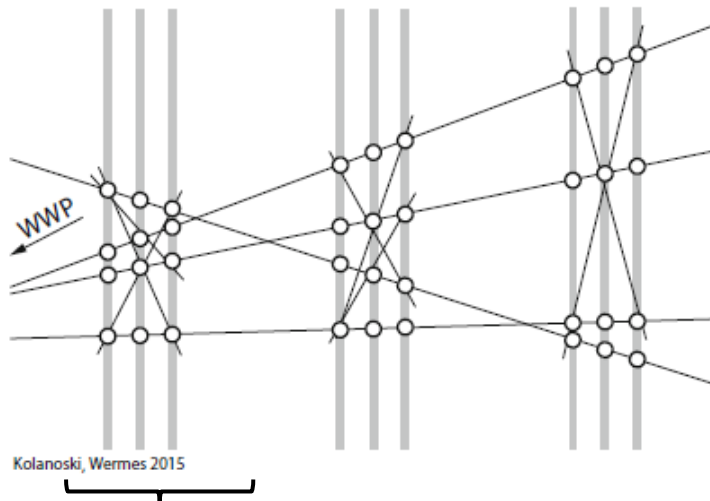


Track reconstruction:

Track reconstruction is usually split into two separate steps:

- **Pattern recognition:** detector hits (space points) are assigned to individual tracks
- **Fit of track model** to space points, accounting for resolution & multiple scattering

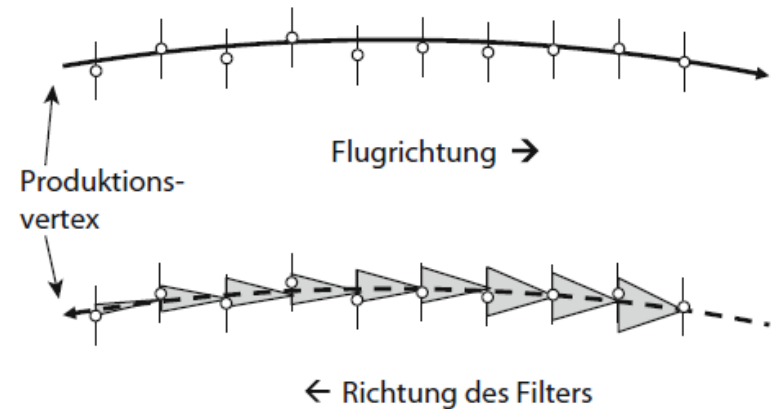
Pattern recognition: here w/ local tracklets



Do locally all possible combinations (tracklets)

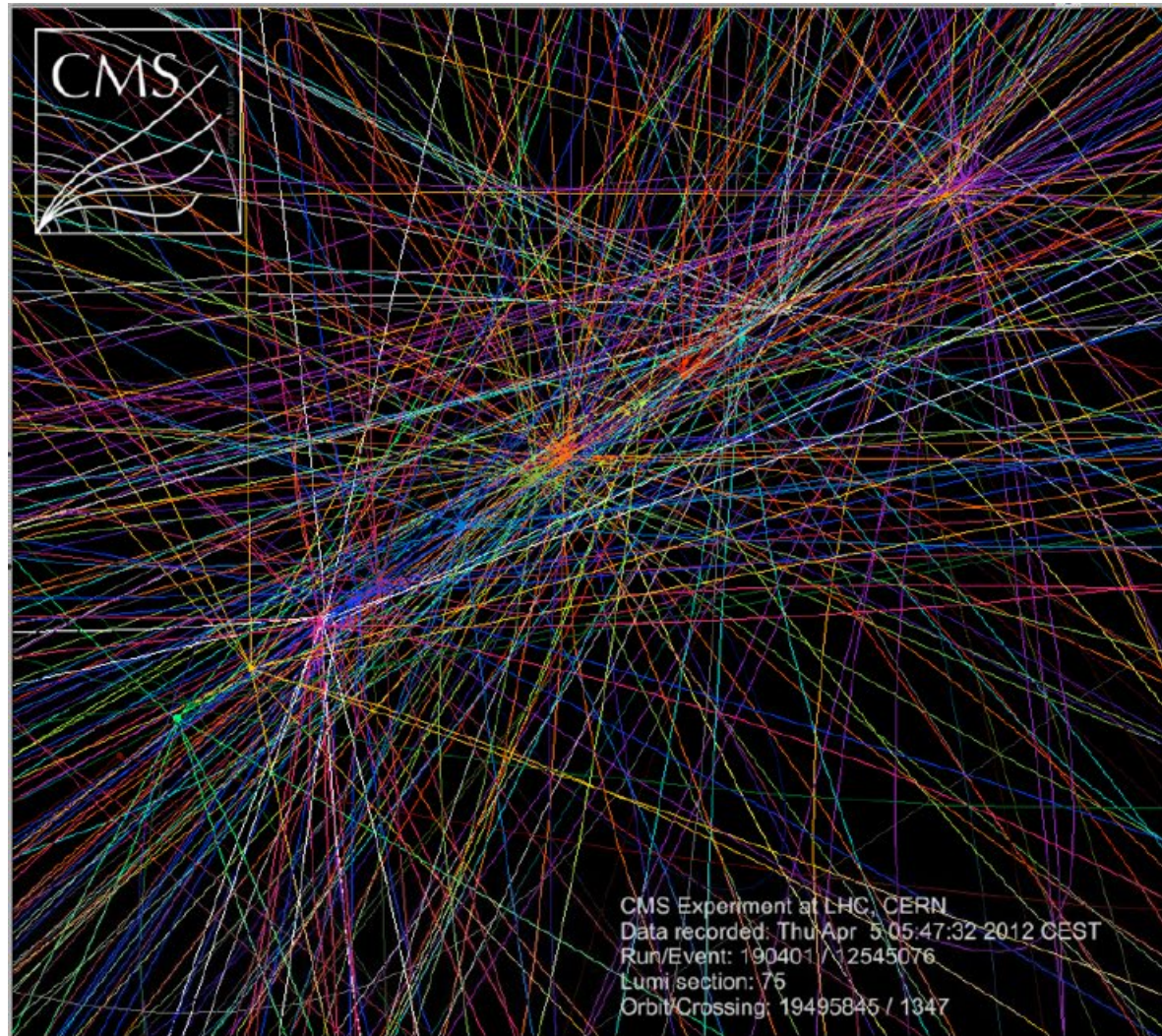
Combine local stubs to global tracks

Fit the hits of tracks by a track model. Often: Kalman filter to consider scattering and refine track model.

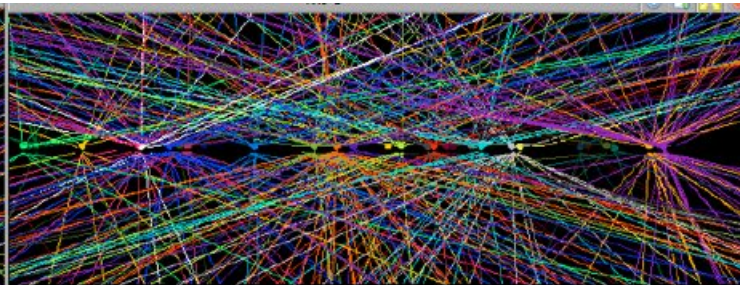


In this way the track model at the last point (close to vertex) is optimized and allows best prediction of vertex.

Tracking detector layout optimized to allow fast and efficient pattern recognition and very good prediction of the vertex from the fitted track model at the last hit. ²⁶



CMS Experiment at LHC, CERN
Data recorded: Thu Apr 5 05:47:32 2012 CEST
Run/Event: 190401 / 12545076
Lumi section: 75
Orbit Crossing: 19495845 / 1347



Rho Phi

